ORIGINAL ARTICLE

An Investigation of Cell Displacement in Direct and Indirect DNA Damage Induced by Photon Radiation: A Geant4-DNA Study

Ali Azizi Ganjgah, Payvand Taherparvar*

Department of Physics, Faculty of Science, University of Guilan, Postal Code 4193833697, Rasht, Iran

*Corresponding Author: Payvand Taherparvar
Email: p.taherparvar@guilan.ac.ir

Received: 23 December 2023 / Accepted: 17 March 2024

Abstract

Purpose: This study aimed to investigate the biological effects of photon radiation and its potential for cancer treatment through targeted radiation therapy by studying direct and indirect DNA damage induced by 15, 30, and 50 keV photon radiation using Geant4-DNA Monte Carlo simulations.

Materials and Methods: Two spherical cells (C and C_2) and their cell nucleus were modeled in liquid water. An atomic DNA model constructed in the Geant4-DNA Monte Carlo simulation toolkit, containing 125,000 chromatin fibers, was placed inside the nucleus of the C_2 cell. The number of direct and indirect Single-Strand Breaks (SSBs), Double-Strand Breaks (DSBs), and hybrid double-strand breaks (HDSB) in the C_2 cell caused by 15, 30, and 50 keV photons were calculated for N_2←CS, N_2←Cy, N_2←C, and N_2←N Target←Source combinations, at the distances of 0, 2.5, and 5 µm between two cells.

Results: Low energy (15 keV) photons emitted within the cell surface and the cell cytoplasm resulted in the highest DNA damage, producing markedly higher SSBs, DSBs, and HDSBs compared to the whole cell and the nucleus sources across 0-5 µm target distances. Increasing the photon energy to 30 and 50 keV showed 81-96% reduced DNA damage. Additionally, the 2.5 µm target distance decreased DSBs up to 53%.

Conclusion: Based on the results, 15 keV photons are more effective for the inhibition or control of cancer cells.

Keywords: Geant4- Deoxyribonucleic Acid; Deoxyribonucleic Acid Damage; Single Strand Breaks; Double Strand Breaks; Hybrid Double Strand Breaks.

PROOF

Copyright © 2025 Tehran University of Medical Sciences.
This work is licensed under a Creative Commons Attribution-NonCommercial 4.0 International license (https://creativecommons.org/licenses/by-nc/4.0/). Noncommercial uses of the work are permitted, provided the original work is properly cited.
DOI:

1. Introduction

Today, common cancer treatments include surgery, chemotherapy, and radiation therapy to kill cancer cells by damaging DNA and inducing cell death. Radiation therapy is used as an effective cancer treatment for over 50% of patients with many types of cancer [1]. Radiation therapy uses direct and indirect ionizing radiation such as gamma, X-rays, electrons, protons, helium beams, and heavier ions to affect target cells to kill cancer cells specifically. Radiation therapy has two principal aims. The first is to deliver a radiation dose to cancer cells in the body to either kill cancer cells or cause genetic changes resulting in cancer cell death. The second is to minimize the damage to the surrounding healthy tissues.

Considering the challenges in achieving the latter approach, opting for targeted internal radiation therapy emerges as an appropriate option [2, 3]. Targeted Radionuclide Therapy (TRT), also known as molecular radiotherapy, is an innovative approach to the radiation therapy techniques. It uses β-radiating radionuclides to specifically affect target cells by disrupting cell cycle and specific signaling pathways, resulting in tumor regression while minimizing damage to the surrounding tissues [4]. Auger Electron-Emitting (AEE) radioisotopes are invaluable tools for delivering the optimal dose selectively to the tumor volume while sparing the healthy tissues. The benefit of using AEs is that they have energies ranging from a few eV to several keV and emit particles with high Linear Energy Transfer (LET) which is significantly lethal on both cellular and sub-cellular scales [5, 6].

Optimizing the effectiveness of the TRT techniques requires an understanding of the interactions of radiation with cells and the biophysical effects of radiation on biological targets. DNA molecules are considered the most vital among the cell constituents due to their role as carriers of genetic information. Thus, it is considered the main component for causing radiation-induced cell death. It is proven that the greater the unrepaired DNA base damage, the higher incidence of lethality. The energy deposition of the ionizing rays causes DNA damage both directly and indirectly via the production of Reactive Oxygen Species (ROS) and other secondary electrons. The types of DNA damage can be usually grouped into Single-Strand Breaks (SSBs) and Double-Strand Breaks (DSBs), which influence the biological effect of exposure to ionizing radiation. While most of these damages can be repaired by DNA repair mechanisms, DSBs are particularly challenging to repair and often result in cell death. Therefore, the DNA within the cell nucleus is considered the primary target for radiation effects, known as "targeted effects" [7]. The study of radiation damage at the molecular scale has garnered much attention in recent years, with micro- and nano-dosimetry tissues serving as valuable tools. Understanding the mechanisms of DNA damage is essential in fully comprehending the biological nature of radiation sensitivity, making it a suitable criterion for investigating the effects of radiation and ion therapy. Interactions created at the molecular scale are highly complex and cannot be evaluated directly via analytical methods.

Today, advanced radiotherapy techniques necessitate the use of theoretical analysis and experimental methods to determine radiation track structure at the nanoscale and assess radiation effects on DNA molecules at the cellular and subcellular levels [8-10]. In this way, many Monte Carlo (MC) simulation reports have been performed as the standard for verification, validation, and development of the radiation dosimetry applications. Recent progress in the MC method made it possible to simulate the radiation transport and interactions as well as the distribution of its energy deposition inside a nucleus, and even more precisely, at the DNA scale. It enables mimicking intricate physical and chemical interactions and radiation-induced DNA damage, making more precise predictions of how radiation would affect living cells biologically [8-10].

Various codes have been developed based on the MC method for accurate and reliable prediction of DNA damage such as Geant4-DNA [11-15], MCNP [16], PENELOPE [17,18], and PARTRAC [19]. Recently, the Geant4-DNA code, besides its wide applications in particle transport, has been widely used in radiobiological applications and Nano dosimetry calculations. The Geant4-DNA, an extension of Geant4, is one of the most advanced and validated codes. It provides a detailed simulation of charged particle transport in liquid water and DNA constituents down to the nanometer scale and can model direct and indirect DNA damages. This code can perform structure-pathway simulations at low energies (about eV) to high energy (MeV) with high accuracy [20].

Since it is important to consider the correct geometry of the object in MC simulation codes, configurations of the DNA model include three categories: linear cylinder model, volumetric model, and atomic model. In the linear model, cylindrical shapes are used to model the DNA structure [20]. In the volumetric model, simple shapes are

PROOF

used to model the bases, sugar-phosphate groups, and other parts of the DNA molecule [21]. In the atomic model, which is also used in this research, the basic atoms that compose DNA are simulated by spheres with van der Waals radius [22, 23]. It is considered a more accurate model than others. The importance of assuming the real model as much as possible for the DNA shape is undeniable in evaluating DNA damages [24].

In this study, the direct and indirect DNA damage caused by photons was calculated using an atomic model, the configuration of which will be described in the Material and Methods section.

2. Materials and Methods

The Geant4-DNA version 11.1.1 has been used to simulate the interaction of particles at the molecular scale. Geant4 is a general-purpose toolkit for simulating the transport of particles through matter in various fields including high energy physics, nuclear physics, space science, and medical physics using MC techniques [15]. Geant4-DNA is specialized in comprehensive physics and chemistry models to simulate the interactions of radiation with geometrical structures of the biological medium. It simulates track structure in liquid water down to the nanometer scale and can model direct and indirect DNA damage.

In the present study, two homogeneous spheres of unit-density liquid water were considered for cell modeling. Based on the typical dimensions for lymphocytes and the V79 Chinese hamster cells [25], the radius of the cell and its nucleus were chosen to be 5 and 4 µm, respectively. Taking the cell nucleus as the target, the monoenergetic photon radiation with energies of 15, 30, and 50 keV were assumed to be uniformly distributed as random emission points-within the whole Cell (C), the Cell Surface (CS), the Cytoplasm (Cy), and the cell Nucleus (N), respectively, to consider all of the source distribution states in the cell [26]. For the evaluation of the cross-dose situation, where the absorbed dose received from emission by decays in the neighboring cell and its effects on the DNA damage, a second similar cell was located in the positive x-axis direction assuming the center of the first one located at the origin of the cartesian coordinate. The distances between two cells were considered 0, 2.5, and 5 µm. In this configuration, the nucleus of the simulated cells is filled with 125,000 chromatin fibers which were randomly distributed in the spherical regions (as shown in Figure 1). Constructing chromatin fiber was performed based on the study by Ahmadi Ganjeh *et al.* [27]. In this way, the nucleotide pair was defined as a base pair (bp), which consists of 63 atoms. The properties of atoms such as chemical element, position, and base of nitrogen are considered based on the information provided by Bernal and co-workers [24]. Following a double helix of 154 bp construction by rotating each bp by +36°, the nucleosome was made by folding two double-helical loops around a sphere (histone). The histone protein has a positive charge that reacts with the phosphate groups of DNA with a negative charge. The histones prevent DNA binding and protect against DNA damage. After the nucleosome, chromatin fiber was made by a helix with 6 nucleosomes, and by repeating this chromatin fiber structure, the cell nucleus was simulated. In the cross-dose case, four configurations were considered for the evaluation of DNA damages: N2←C, N2←CS, N2←N, and N2←Cy. In all of the simulation stages, N2 (the nucleus of cell C2) was selected as the target. A visualization of the simulated model is provided in Figure 2.

For assessing DNA damges, direct and indirect SSB, DSB, and HDSB were evaluated in this research. An energy threshold of 8.22 eV was utilized for the Physical and Chemical stages as recommended in the literature [27]. Indirect damage (chemical stage) produced radicals and molecules including H_2O_2, H_2, H, H+, OH-, OH, and eaq- in water. OH (hydroxyl) has the greatest capacity to interact with DNA [28]. The hydroxyl radical interacts with sugar and base groups in DNA more than others. The probability of strand break production in the DNA by hydroxyl radicals is 13% [8]. If the energy deposited in the DNA exceeds the threshold value of 8.22 eV, SSBs will occur. DSB is counted when two SSBs happen on the two strands with a distance of less than 10 base pairs. Moreover, HDSB is counted when two SSBs happen (one SSB directly and one SSB indirectly) on the two strands with a distance of less than 10 base pairs (bp). The G4EmDNAPhysics_option6 [29] and G4EmDNAChemistry_option3 [30] physics lists were applied to simulate the physical and chemical stages, respectively. The G4EmDNAPhysics_option6 is a physics model for simulation of electron transport in liquid water over an energetic range of 11 eV to 256

PROOF

keV [31]. Photon interactions are based on the Livermore/EADL97 physics models in G4EmDNAPhysics_option6 [32]. In this study, although the primary radiation source is photons, the focus is on accurate secondary electrons produced through the initial photon interactions. For electron transport, electrons below a cut-off kinetic energy of 11 eV are stopped and their remaining kinetic energy is deposited at the same point. The default chemical reactions and the corresponding reaction rates are presented in Table 1. The number of primary particles simulated was 5 ×108 photons and the statistical error in the results was less than 1%.

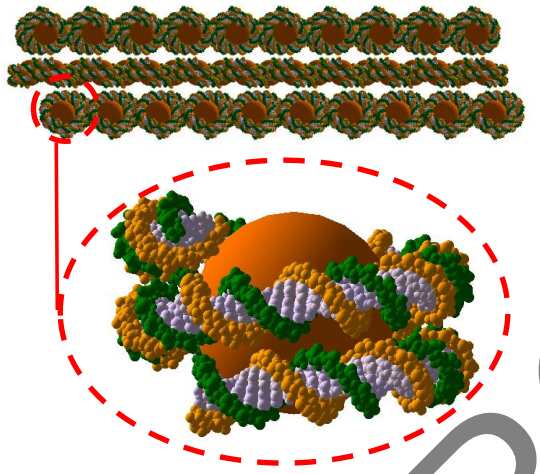

Figure 1. 3D view of a chromatin fiber consists of 10 sets of fragments

Table 1. Implemented chemical reactions and reaction rates in the default "G4EmDNAChemistry" constructor used in Geant4-DNA [33]

Chemical reaction	Reaction rate (10^{10} M^{-1} s^{-1})
$e^-_{aq} + e^-_{aq} + 2H_2O \rightarrow H_2 + 2OH^-$	0.5
$e^-_{aq} + H° + H_2O \rightarrow H_2 + OH^-$	2.65
$e^-_{aq} + °OH \rightarrow OH^-$	2.95
$e^-_{aq} + H_3O^+ \rightarrow H° + H_2O$	2.11
$e^-_{aq} + H_2O_2 \rightarrow OH^- + °OH$	1.41
$°OH + °OH \rightarrow H_2O_2$	0.44
$°OH + H° \rightarrow H_2O$	1.44
$H° + H° \rightarrow H_2$	1.2
$H_3O^+ + OH^- \rightarrow 2H_2O$	14.33

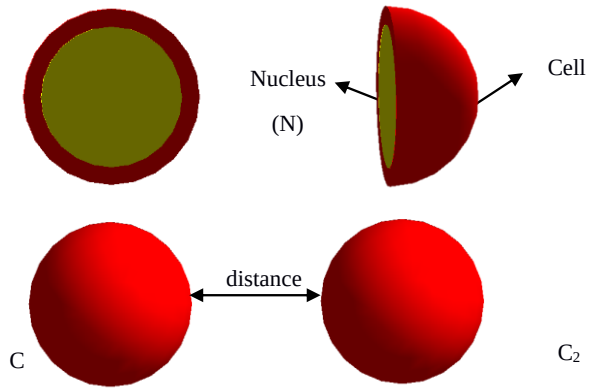

Figure 2. OpenGL Visualization of the spherical geometry of a simulated cell using the Geant4-DNA toolkit. The cell has a radius of 5 µm shown in red, with a nucleus of 4 µm radius depicted in yellow

3. Results

To verify our simulation modeling, the direct SSBs and DSBs of the atomic DNA model irradiated with 50-200 keV electron beams (in 50 keV steps) in the absence of nanoparticle were compared with the values reported by Santiago *et al* [34]. The total strand breaks reported by Santiago *et al.* were 2228, 1288, 1062, and 922 in the energy values of 50, 100, 150, anf and 200 keV, respectively. Our simulation results for the total strand breaks were 2423, 1383, 1010, and 850 in the energy range of 50-200 keV (in 50 keV steps) of electron beams, respectively. Comparison between the results show a good agreement between our results and the corresponding literature with average differences about 7%.

The number of SSBs and DSBs induced by 15, 30, and 50 keV photons at distances from 0 to 5 µm are shown in Table 2, for N_2←CS, N_2←Cy, N_2←C, and N_2←N Target←Source combinations.

Results for 2.5 µm distance between two cells show that the SSB (DSB) decreased by 39% (19%), 38% (15%), and 47% (48%) for the N_2←CS for 15, 30, and 50 keV of photon energies, respectively, compared to the closest distance of two cells (0 µm).

PROOF

Table 2. Number of SSBs and DSBs (Direct and Indirect) induced by 15, 30, and 50 keV photons for the following Target←Source combinations: N_2←CS, N_2←Cy, N_2←C, and N_2←N

Target ← Source	Energy (keV)	0 µm	2.5 µm	5 µm
SSB (N_2 ← CS)	15	5734	3466	2274
SSB (N_2 ← Cy)	15	5624	3452	2270
SSB (N_2 ← C)	15	5603	3422	2246
SSB (N_2 ← N)	15	5514	3209	2160
SSB (N_2 ← CS)	30	778	478	299
SSB (N_2 ← Cy)	30	747	466	278
SSB (N_2 ← C)	30	736	455	272
SSB (N_2 ← N)	30	604	281	208
SSB (N_2 ← CS)	50	472	250	218
SSB (N_2 ← Cy)	50	400	238	205
SSB (N_2 ← C)	50	347	201	172
SSB (N_2 ← N)	50	337	169	78
DSB (N_2 ← CS)	15	506	408	250
DSB (N_2 ← Cy)	15	487	328	196
DSB (N_2 ← C)	15	472	293	184
DSB (N_2 ← N)	15	453	283	182
DSB (N_2 ← CS)	30	73	62	41
DSB (N_2 ← Cy)	30	64	44	23
DSB (N_2 ← C)	30	64	43	14
DSB (N_2 ← N)	30	42	26	11
DSB (N_2 ← CS)	50	58	30	19
DSB (N_2 ← Cy)	50	47	27	16
DSB (N_2 ← C)	50	28	16	12
DSB (N_2 ← N)	50	25	15	11

PROOF

These values were 38% (32%), 37% (31%), and 40% (42%) for the N_2←Cy, 39% (38%), 38% (33%), and 42% (43%) for the N_2←C, and 42% (37%), 53% (38%), and 50% (40%) for the N_2←N configuration.

Results for 5 µm distance show that the SSB (DSB) decreased by 60% (50%), 61% (44%), and 54% (67%) for the N_2←CS, 59% (60%), 63% (64%), and 49% (66%) for the N_2←Cy, 60% (61%), 63% (78%), and 50% (51%) for the N_2←C, and 61% (60%), 65% (74%), and 77% (56%) for the N_2←N, for 15, 30, and 50 keV photon energies, respectively.

Furthermore, when comparing the SSB (DSB) induced by 15 keV photons at the closest cell distance (0 µm) to those induced by 30 and 50 keV photons, there were significant decreases observed. Specifically, the SSB (DSB) reductions for N_2←CS were 86% (85%) and 92% (88%), for N_2←Cy were 87% (87%) and 93% (90%), for N_2←C were 87% (86%) and 94% (94%), and for N_2←N were 89% (91%) and 94% (94%), respectively.

These values for 2.5 µm distance between two cells were 86% (85%), and 93% (92%) for N_2←CS, 86% (86%), and 93% (92%) for N_2←Cy, 87% (85%), and 94% (94%) for N_2←C, and 91% (91%), and 95% (94%) for N_2←N, respectively.

The results at 5 µm distance between two cells showed decreases of 79% (75%), and 90% (92%) for

the N_2←CS, 79% (77%), and 91% (92%) for the N_2←Cy, 79% (76%), and 92% (93%) for the N_2←C, and 87% (86%), and 96% (94%) for the N_2←N, respectively.

The number of HDSBs induced by 15, 30, and 50 keV photons at distances from 0 to 5 µm are shown in Table 3 for N_2←CS, N_2←Cy, N_2←C, and N_2←N Target←Source combinations. Compared to the closest distance between the two cells (0 µm), the HDSB at 2.5 µm decreased for the N_2←CS by 25%, 21%, and 20% with 15, 30, and 50 keV photons, respectively. For the N_2←Cy, the decrease was 37%, 70%, and 50%, for the N_2←C, it was 34%, 67%, and 75%, and for the N_2←N, it was 52%, 33%, and 100%, respectively. At 5 µm, the HDSB in the case of N_2←CS decreased by 56%, 64%, and 40% for 15, 30, and 50 keV photons, respectively. For N_2←Cy decreased by 61%, 80%, and 50%, for N_2←C decreased by 67%, 100%, and 100%, and for N_2←N decreased by 72%, 100%, and 100%.

Furthermore, compared to 15 keV photons the HDSB for 30 (50) keV photons at 0 µm decreased for the N_2←CS by 81% (93%), for the N_2←Cy by 86% (94%), for the N_2←C by 91% (94%), and for the N_2←N by 95% (95%), respectively. At 2.5 µm, the decreases were 80% (93%) for N_2←CS, 93% (95%) for N_2←Cy, 95% (98%) for N_2←C, and 93% (100%) for N_2←N, respectively. At 5 µm, decreased by 85% (91%) for the N_2←CS, decreased by 93% (93%) for the N_2←Cy, decreased by 95% (100%) for the N_2←C, and decreased by 100% (100%) for the N_2←N, respectively.

Moreover, results in Table 4 demonstrate that as the energy of the incident photon photons decreases, the total number of interactions increases, which are in agreement with the results of Lara *et al.* [35]. This correlation is due to the energy dependence of the photoelectric effect, which is the dominant interaction mechanism for low-energy photons. Lower energy photon beams are more likely to undergo photoelectric absorption events rather than penetrate deeper into the target volume. Therefore, photoelectric absorption rate at lower energies increases which leads to an increased production of secondary electrons, subsequently resulting in heightened levels of ionization, excitation, and cascading (indirect) damage effects.

4. Discussion

The results of this study clearly demonstrate that 15 keV photon irradiation causes substantially more DNA damage compared to the other higher energy photons in all Target←Source combinations. The significant inverse relationship observed between photon energy and resulting SSBs, DSBs, and HDSBs can be attributed to the particle range and local energy deposition patterns. Lower energy 15 keV photons have very short penetrating ranges in liquid

PROOF

Table 3. Number of HDSBs induced by 15, 30, and 50 keV photons for the following Target←Source combinations: N_2←CS, N_2←Cy, N_2←C, and N_2←N

Target ← Source	Energy (keV)	0 µm	2.5 µm	5 µm
HDSB (N_2 ← CS)	15	75	56	33
HDSB (N_2 ← Cy)	15	72	45	28
HDSB (N_2 ← C)	15	67	44	22
HDSB (N_2 ← N)	15	65	31	18
HDSB (N_2 ← CS)	30	14	11	5
HDSB (N_2 ← Cy)	30	10	3	2
HDSB (N_2 ← C)	30	6	2	1
HDSB (N_2 ← N)	30	3	2	0
HDSB (N_2 ← CS)	50	5	4	3
HDSB (N_2 ← Cy)	50	4	2	2
HDSB (N_2 ← C)	50	4	1	0
HDSB (N_2 ← N)	50	3	0	0

Table 4. The table presents the number of photoelectric interactions induced by primary photons, giving rise to secondary electrons that cause ionization and excitation

Interactions	Energy (keV)	Distance (μm)	$N_2 \leftarrow CS$	$N_2 \leftarrow Cy$	$N_2 \leftarrow C$	$N_2 \leftarrow N$
photoelectric	15	0	1.7×10^5	1.6×10^5	1.59×10^5	1.5×10^5
photoelectric	30	0	1.77×10^4	1.75×10^4	1.71×10^4	1.62×10^4
photoelectric	50	0	3.2×10^3	3×10^3	2.9×10^3	2.7×10^3
Ionisation	15	0	6.85×10^7	6.24×10^7	6.24×10^7	6.23×10^7
Ionisation	30	0	5×10^6	4.38×10^6	4.33×10^6	4.21×10^6
Ionisation	50	0	4.5×10^6	4.37×10^6	4.32×10^6	4.13×10^6
Excitation	15	0	9.79×10^6	9.79×10^6	8.98×10^6	8.96×10^6
Excitation	30	0	7.2×10^5	6.3×10^5	6.25×10^5	6.17×10^5
Excitation	50	0	6.32×10^5	6.26×10^5	6.01×10^5	6×10^5
photoelectric	15	2.5	1.2×10^5	1.06×10^5	1.01×10^5	9.51×10^4
photoelectric	30	2.5	1.09×10^4	1.09×10^4	1.05×10^4	9.7×10^3
photoelectric	50	2.5	2.2×10^3	2.1×10^3	2×10^3	1.9×10^3
Ionisation	15	2.5	4.19×10^7	3.99×10^7	3.88×10^7	3.76×10^7
Ionisation	30	2.5	3.01×10^6	2.95×10^6	2.67×10^6	2.64×10^6
Ionisation	50	2.5	2.61×10^6	2.6×10^6	2.29×10^6	2.28×10^6
Excitation	15	2.5	5.96×10^6	5.74×10^6	5.54×10^6	5.37×10^6
Excitation	30	2.5	4.29×10^5	4.18×10^5	3.93×10^5	3.82×10^5
Excitation	50	2.5	3.74×10^5	3.71×10^5	3.3×10^5	3.3×10^5
photoelectric	15	5	7.01×10^4	6.82×10^4	6.7×10^4	6.48×10^4
photoelectric	30	5	7.6×10^3	7.04×10^3	6.9×10^3	6.8×10^3
photoelectric	50	5	1.6×10^3	1.5×10^3	1.01×10^3	1×10^3
Ionisation	15	5	2.85×10^7	2.73×10^7	2.72×10^7	2.48×10^7
Ionisation	30	5	2.08×10^6	2.05×10^6	1.77×10^6	1.58×10^6
Ionisation	50	5	1.95×10^6	1.63×10^6	1.59×10^6	1.47×10^6
Excitation	15	5	4.04×10^6	3.95×10^6	3.89×10^6	3.56×10^6
Excitation	30	5	2.95×10^5	2.95×10^5	2.63×10^5	2.52×10^5
Excitation	50	5	2.75×10^5	2.39×10^5	2.34×10^5	2.22×10^5

PROOF

water, interacting within a small radius of their emission source to produce dense ionization events that directly or indirectly damage proximal DNA molecules. Since 30 and 50 keV photons have longer ranges, dispersing absorbed dose over larger cellular volumes and interacting with fewer DNA fragments near their origin to cause less clustered damage. In addition to particle energy, the localization of the photon source also critically impacted DNA damage yields. Emissions originating on the Cell Surface (CS) or the cell cytoplasm (Cy) resulted in 25-94% more DSBs than the whole cell (C) or the nucleus (N). This again reflects very short-range energy deposition patterns for the low-energy photons simulated. N and C compartment emissions would produce dense ionization around closely packed DNA molecules, while photons emitted from Cy or CS would interact with DNA less frequently. The decline in DNA damage observed over short 2.5-5 μm distances between source and target further indicates the importance of proximity and localized energy deposition at the nanometer scale. Appreciable DSB reductions of up to 53% over just a few μm emphasize that even minor changes in cellular geometry can influence biological outcomes for low-energy photon sources. This sensitivity likely arises from the very limited particle ranges failing to bridge small gaps between nearby cells. Similar interactions in tumor

contexts could modulate therapeutic effects on malignant versus normal cells based on their relative locations.

Overall, the modeled DNA damage patterns demonstrated that localized, low-energy photon emissions produce the greatest direct biological impacts, with damage falling sharply over small distances. These results highlight the importance of micro dosimetry considerations and nanoscale energy deposition phenomena in evaluating potential photon therapies.

5. Conclusion

In this research, Geant4-DNA was utilized to calculate direct and indirect DNA damage caused by monoenergetic photons with energies of 15, 30, and 50 keV. The study established the relationships between photon energy, the target distance, and resulting DNA damage, including SSBs, DSBs, and HDSBs at distances of 0-5 µm from the DNA target. The 15 keV monoenergetic photons produced the highest and 50 keV monoenergetic photons lowest number of DNA strand breaks, respectively. Analyses of SSBs, DSBs, and HDSBs at varying distances revealed a strong distance dependence so that DNA damage decreased rapidly from 0 to 5 µm. Additionally, the (N2←CS) source-target combination resulted in higher DNA damage compared to other configurations. The DNA damage quantification and cell distance effects presented provide insights into photon therapy effectiveness and guide optimization of delivery strategies for targeted cancer treatment.

PROOF

Acknowledgment

The authors received no financial support for the publication of this article.

References

1- R. Salim and P. Taherparvar, “Monte Carlo single-cell dosimetry using Geant4-DNA: the effects of cell nucleus displacement and rotation on cellular S values,” *Radiation and Environmental Biophysics*, vol. 58, pp. 353-371, (2019).

2- P. Taherparvar, and A. Azizi Ganjgah, “Comparison of direct DNA damage by protons and oxygen, carbon, and helium ions using Geant4-DNA code,” *Iranian Journal of Physics Research*, vol. 23, no. 4, pp. 353-371, (2024).

3- R. Baskar, J. Dai, N. Wenlong, R. Yeo, and K.-W. Yeoh, “Biological response of cancer cells to radiation treatment,” *Frontiers in molecular biosciences*, vol. 1, p. 24, (2014).

4- S. Asadian *et al.*, “β-radiating radionuclides in cancer treatment, novel insight into promising approach,” *Pharmacological research*, vol. 160, p. 105070, (2020).

5- M. S. Moradi and B. S. Bidabadi, “Micro-dosimetry calculation of Auger-electron-emitting radionuclides mostly used in nuclear medicine using GEANT4-DNA,” *Applied Radiation and Isotopes*, vol. 141, pp. 73-79, (2018).

6- J.-P. Pouget *et al.*, “Cell membrane is a more sensitive target than cytoplasm to dense ionization produced by auger electrons,” *Radiation research*, vol. 170, no. 2, pp. 192-200, (2008).

7- H. Date, K. Sutherland, H. Hasegawa, and M. Shimozuma, “Ionization and excitation collision processes of electrons in liquid water,” *Nuclear Instruments and Methods in Physics Research Section B: Beam Interactions with Materials and Atoms*, vol. 265, no. 2, pp. 515-520, (2007).

8- P. Ahmadi, M. S. Zafarghandi, and A. Shokri, “Calculation of direct and indirect damages of Auger electron-emitting radionuclides based on the atomic geometric model: A simulation study using Geant4-DNA toolkit,” *Nuclear Instruments and Methods in Physics Research Section B: Beam Interactions with Materials and Atoms*, vol. 483, pp. 22-28, (2020).

9- L. H. Thompson, “Recognition, signaling, and repair of DNA double-strand breaks produced by ionizing radiation in mammalian cells: the molecular choreography,” *Mutation Research/Reviews in Mutation Research*, vol. 751, no. 2, pp. 158-246, (2012).

10- M. Frankenberg-Schwager and D. Frankenberg, “DNA double-strand breaks: their repair and relationship to cell killing in yeast,” *International journal of radiation biology*, vol. 58, no. 4, pp. 569-575, (1990).

11- M. A. Bernal *et al.*, “Track structure modeling in liquid water: A review of the Geant4-DNA very low energy extension of the Geant4 Monte Carlo simulation toolkit,” *Physica Medica*, vol. 31, no. 8, pp. 861-874, (2015).

12- Z. Francis *et al.*, “Molecular scale track structure simulations in liquid water using the Geant4-DNA Monte-Carlo processes,” *Applied radiation and isotopes*, vol. 69, no. 1, pp. 220-226, (2011).

13- J. Allison *et al.*, “Recent developments in Geant4,” *Nuclear instruments and methods in physics research section A: Accelerators, Spectrometers, Detectors and Associated Equipment*, vol. 835, pp. 186-225, (2016).

14- R. Salim, and P. Taherparvar, “A Monte Carlo study on the effects of a static uniform magnetic field on micro-scale dosimetry of Auger-emitters using Geant4-DNA,” Radiation Physics and Chemistry, vol. 195, pp. 110063, 2022.

15- R. Salim, and P. Taherparvar, "Dosimetry assessment of theranostic Auger-emitting radionuclides in a micron-sized multicellular cluster model: a Monte Carlo study using Geant4-DNA simulations," Applied Radiation and Isotopes, vol. 188, pp. 110380, 2022.

16- U. Titt, B. Bednarz, and H. Paganetti, "Comparison of MCNPX and Geant4 proton energy deposition predictions for clinical use," *Physics in Medicine & Biology*, vol. 57, no. 20, p. 6381, (2012).

17- M. Bernal and J. Liendo, "An investigation on the capabilities of the PENELOPE MC code in nanodosimetry," *Medical physics*, vol. 36, no. 2, pp. 620-625, (2009).

18- J. Baró, J. Sempau, J. Fernández-Varea, and F. Salvat, "PENELOPE: an algorithm for Monte Carlo simulation of the penetration and energy loss of electrons and positrons in matter," *Nuclear Instruments and Methods in Physics Research Section B: Beam Interactions with Materials and Atoms*, vol. 100, no. 1, pp. 31-46, (1995).

19- W. Friedland, P. Jacob, and P. Kundrat, "Mechanistic simulation of radiation damage to DNA and its repair: on the track towards systems radiation biology modelling," *Radiation protection dosimetry*, vol. 143, no. 2-4, pp. 542-548, (2011).

20- L. Lindborg and H. Nikjoo, "Microdosimetry and radiation quality determinations in radiation protection and radiation therapy," *Radiation protection dosimetry*, vol. 143, no. 2-4, pp. 402-408, (2011).

21- G. Raisali, L. Mirzakhanian, S. F. Masoudi, and F. Semsarha, "Calculation of DNA strand breaks due to direct and indirect effects of Auger electrons from incorporated 123I and 125I radionuclides using the Geant4 computer code," *International journal of radiation biology*, vol. 89, no. 1, pp. 57-64, (2013).

22- Z. A. Ganjeh, M. Eslami-Kalantari, M. E. Loushab, and A. A. Mowlavi, "Simulation of direct DNA damages caused by alpha particles versus protons," Nuclear Instruments and Methods in Physics Research Section B: Beam Interactions with Materials and Atoms, vol. 473, pp. 10-15, 2020.

23- J. Chen, S. Yun, T. Dong, Z. Ren, and X. Zhang, "Investigate the radiation-induced damage on an atomistic DNA model by using Geant4-DNA toolkit," *Nuclear Instruments and Methods in Physics Research Section B: Beam Interactions with Materials and Atoms*, vol. 494, pp. 59-67, (2021).

24- M. A. Bernal *et al.*, "An atomistic geometrical model of the B-DNA configuration for DNA–radiation interaction simulations," *Computer Physics Communications*, vol. 184, no. 12, pp. 2840-2847, (2013).

25- C. Bousis, D. Emfietzoglou, P. Hadjidoukas, and H. Nikjoo, "Monte Carlo single-cell dosimetry of Auger-electron emitting radionuclides," *Physics in Medicine & Biology*, vol. 55, no. 9, p. 2555, (2010).

26- Y.-Y. Hsiao, F.-C. Tai, C.-C. Chan, and C.-C. Tsai, "A computational method to estimate the effect of gold nanoparticles on X-ray induced dose enhancement and double-strand break yields," *IEEE Access*, vol. 9, pp. 62745-62751, (2021).

27- Z. A. Ganjeh, M. Eslami-Kalantari, M. E. Loushab, and A. A. Mowlavi, "Calculation of direct DNA damages by a new approach for carbon ions and protons using Geant4-DNA," *Radiation Physics and Chemistry*, vol. 179, p. 109249, (2021).

28- S. Siddique and J. C. Chow, "Recent advances in functionalized nanoparticles in cancer theranostics," *Nanomaterials*, vol. 12, no. 16, p. 2826, (2022).

29- S. A. Zein *et al.*, "Monte Carlo simulations of electron interactions with the DNA molecule: A complete set of physics models for Geant4-DNA simulation toolkit," *Nuclear Instruments and Methods in Physics Research Section B: Beam Interactions with Materials and Atoms*, vol. 542, pp. 51-60, (2023).

30- N. Lampe, M. Karamitros, V. Breton, J. M. Brown, D. Sakata, D. Sarramia, and S. Incerti, "Mechanistic DNA damage simulations in Geant4-DNA Part 2: Electron and proton damage in a bacterial cell," *Physica Medica*, vol. 48, pp. 146-155, (2018).

31- M. Bordage, J. Bordes, S. Edel, M. Terrissol, X. Franceries, M. Bardiès, N. Lampe, and S. Incerti, "Implementation of new physics models for low energy electrons in liquid water in Geant4-DNA," *Physica Medica*, vol. 32, no. 12, pp. 1833-1840, (2016).

32- D. E. Cullen, J. H. Hubbell, and L. Kissel, "EPDL97: the Evaluated Photon Data Library, "97 Version, 1997," *University of California, Lawrence Livermore National Laboratory: Livermore, CA*, (1997).

33- I. Kyriakou, D. Sakata, H. N. Tran, Y. Perrot, W.-G. Shin, N. Lampe, S. Zein, M. C. Bordage, S. Guatelli, and C. Villagrasa, "Review of the Geant4-DNA simulation toolkit for radiobiological applications at the cellular and DNA level," *Cancers*, vol. 14, no. 1, pp. 35, (2021).

34- C. A. Santiago, and J. C. Chow, "Variations in Gold Nanoparticle Size on DNA Damage: A Monte Carlo Study Based on a Multiple-Particle Model Using Electron Beams," Applied Sciences, vol. 13, no. 8, pp. 4916, (2023).

35- A. Azizi Ganjgah, and P. Taherparvar, "Evaluation of direct and indirect DNA Damage under the Photon Irradiation in the Presence of Gold, Gadolinium, and Silver Nanoparticles Using Geant4-DNA," *Radiation Physics and Engineering*, vol. 5, no. 3, pp. 33-41, (2024).

PROOF